Evolution of Atmospheric O_2 Through the Phanerozoic, Revisited

Benjamin J. W. Mills[1*], Alexander J. Krause[2*], Ian Jarvis[3] and Bradley D. Cramer[4].

[1]School of Earth and Environment, University of Leeds, LS2 9JT, UK

[2]Department of Earth Sciences, University College London, London WC1E 6BT, UK

[3]Dept. of Geography, Geology and the Environment, Kingston University London, Penrhyn Road, Kingston upon Thames KT1 2EE, UK

[4]Department of Earth and Environmental Sciences, University of Iowa, Iowa City, IA 52242, USA

Corresponding author email: b.mills@leeds.ac.uk , a.krause@ucl.ac.uk

Key words: Oxygen, Phanerozoic, Carbon cycle, Geochemistry, Evolution, Animals

Abstract

An oxygen-rich atmosphere is essential for complex animals. The early Earth had an anoxic atmosphere, and understanding the rise and maintenance of high O_2 levels is essential for investigating what drove our own evolution, and for assessing the likely habitability of exoplanets. A growing number of techniques aim to reproduce changes in O_2 levels over the Phanerozoic Eon (the last 539 Million years). We assess these methods and attempt to draw the reliable techniques together to form a consensus Phanerozoic O_2 curve. We conclude that

O_2 probably made up around 5–10% of the atmosphere during the Cambrian, and rose in pulses to ~15–20% in the Devonian, reaching a further peak of >25% in the Permo-Carboniferous before declining towards the present day. Evolutionary radiations in the Cambrian and Ordovician appear consistent with an oxygen driver, and the Devonian age of the fishes coincides with oxygen rising above 15% atm.

Contents

1. The importance of oxygen

All free-living animals and plants require molecular oxygen (O_2) to perform aerobic respiration. This places atmospheric oxygen at the heart of discussions about what has driven the evolution of Earth's biosphere and more generally, about the potential for intelligence to have developed elsewhere in the universe. The early Earth was devoid of oxygen, but levels in the atmosphere and oceans have risen over time (Farquhar et al., 2000; Lyons et al., 2014). The first animals lived in the ocean and evolved in the Ediacaran period (Wood et al., 2019), about 570 million years ago (Ma), indicating that marine oxygen levels were sufficient to support their metabolisms by this time. During the following Cambrian period (538.8 – 486.9 Ma) life radiated explosively (Erwin et al., 2011), establishing almost all of the modern phyla (the highest subdivision of the kingdom of animals). The principal drivers of the Ediacaran and Cambrian radiations are still debated, but certainly the O_2 metabolic thresholds must have been crossed at some point prior to these evolutionary events (Sperling et al., 2013; Wood et al., 2019). Pulses of rapid animal evolution and extinction continued throughout the Phanerozoic,

and the mass extinction events in the late Ordovician (~445 Ma), Permian–Triassic (~252 Ma) and Triassic–Jurassic (~200 Ma) are convincingly linked to expansions of marine anoxia (waters lacking oxygen; Ahm et al., 2017; He et al., 2020; Wignall and Twitchett, 1996). However, the overall interplay between the volume of oxygenated water and animal evolution over the Phanerozoic remains uncertain – largely because the concentration of oxygen in the atmosphere and oceans over geological time is not well known.

When considering the evolution of intelligence, a useful question is, 'What is the earliest point in Earth history during which humans could have survived on Earth's surface?'. The answer would give an indication of what kind of biosphere was needed on our planet to support intelligence as we know it, and therefore what evolutionary advances might be needed for intelligence to arise on an exoplanet. Currently, the highest altitude of long-term human colonisation is on the Tibetan Plateau at around 4500 m, where the density of the atmosphere is around 60% of that at sea level. The partial pressure of oxygen experienced here is equivalent to being at sea level on a planet with only ~12.5% O_2 in its atmosphere. A selection of metabolic traits acquired over the last >6000 years of permanent human habitation of the plateau (Horscroft et al., 2017) have made complex, intelligent life here possible. This level of atmospheric oxygen abundance is roughly what is thought to be required for oxygen to penetrate deep into the ocean interior (Canfield, 1998). Thus, given that our main constraint on pre-Silurian atmospheric oxygen levels is the persistence of marine anoxia (Sperling et al., 2015), it is possible that an atmospheric oxygen concentration sufficient for highly adapted modern humans may have been available throughout the entire Phanerozoic and perhaps even into the Proterozoic.

Fully resolving the questions around how O_2 levels have influenced animal evolution, and at what stage animals, including humans, might have been able to colonise the Earth, requires more detailed tools for tracking atmospheric oxygen levels through Phanerozoic time.

In this review we will: give an overview of the global oxygen cycle; discuss the currently available methods to track and reconstruct Phanerozoic O_2 levels; and attempt to produce a general consensus view supported by the most reliable methods.

2. What controls O_2 levels in the atmosphere and ocean?

It is possible to produce molecular oxygen when water or carbon dioxide molecules are split by the sun's rays in the upper atmosphere (photolysis), which is why Mars's very thin atmosphere has an O_2 mixing ratio of about 0.17% (Franz et al., 2017). The build-up of an ozone layer during the Paleoproterozoic Era would have curtailed this process, and the only other way to produce large amounts of molecular oxygen is through biological means: oxygenic photosynthesis. Photosynthesis has been active on Earth for at least 2.7 billion years, and perhaps much longer (Buick, 2008), and has produced effectively all of the oxygen that is in the atmosphere and oceans today. However, the accumulation of O_2 in the atmosphere is not simply a matter of determining rates of photosynthesis. As shown in Figure 1, almost all of the oxygen generated through photosynthesis (more than 99%) is consumed rapidly during aerobic respiration (e.g. Hedges and Keil, 1995). In the ocean, organic material is constantly produced through photosynthesis and is respired as it sinks through the water column. This results in oxygen minimum zones (or 'dead zones') where the oxygen demand for respiration reduces the oxygen availability in the water column. On land, plants themselves respire the O_2 they produce, as do the soil communities. However, neither of these environments allows for the complete respiration of all the organic matter initially produced, resulting in the burial and preservation of organic carbon.

The tiny fraction of organic carbon that is buried is responsible for the rise of oxygen to modern levels (Garrels and Perry, 1974). During photosynthesis, one mole of O_2 is produced when converting one mole of CO_2 to organic material, thus every mole of organic carbon that is preserved represents one mole of O_2 which remains free in the surface environment. This

picture is complicated by other processes which occur in the sediments or soils once oxygen has been consumed. Microbes do not need to use aerobic respiration to derive energy from organic matter and may instead process the organic carbon through other avenues, e.g. sulfate reduction, where the 'terminal electron acceptor' (i.e. the molecule where the oxygen is coming from) is SO_4, rather than O_2. In this way the organic carbon is converted to CO_2 and not buried, but no O_2 has been consumed. Fortunately, for the purpose of tracking O_2 fluxes, sulfate reduction produces hydrogen sulfide which readily reacts with iron to form pyrite, and thus every mole of pyrite sulfur buried in sediments represents ~2 moles of photosynthetic O_2 that remains in the surface environment. There are, of course, other consumption fluxes of O_2 aside from respiration, and in the 'long-term' carbon cycle the net O_2 source linked to carbon and pyrite burial is matched by the sinks through oxidation of fossil organic carbon or pyrite sulfur in ancient sediments, either directly during exposure and weathering, or through metamorphism (Garrels and Perry, 1974; Berner, 2004). Several methods for reconstructing atmospheric oxygen abundance rely on reconstructing these sources and sinks of O_2. Others use information that pertains directly to the atmospheric O_2 concentration, to the marine O_2 concentration, or to other aspects of the global carbon cycle which are linked to O_2.

3. Long-term O_2 constraints

Before we assess the Phanerozoic record of atmospheric oxygen, we summarise the wider context of the rise in atmospheric O_2 over Earth history, as this sets key boundaries for any Phanerozoic reconstruction. Figure 2 shows the key long-term constraints on atmospheric O_2 levels. Before the Great Oxidation Event (GOE) during 2400–2200 Ma, atmospheric oxygen concentrations were less than 1 ppm, which is known with some certainty because of abundant evidence for the 'mass-independent fractionation' of sulfur isotopes (MIF-S) in all samples before 2400 Ma (Farquhar et al., 2000). Usually processes that separate isotopes of an

element do so in ways related to the mass of each isotope, but some photochemical atmospheric reactions (i.e. using UV radiation from the Sun) can produce mass-independent effects and are only possible in an atmosphere almost completely devoid of oxygen (Gregory et al., 2021). This explanation is further supported by a plethora of redox sensitive tracers which determined the weathering zone and shallow marine environment to be largely devoid of oxygen at this time (Catling and Zahnle, 2020) and also by marine redox tracers which show that oxygen penetration into the marine environment increases at the time when the MIF-S record disappears (Poulton et al., 2021).

From about 2200 Ma through to the Cambrian, an upper limit on oxygen levels of about 12% of the atmosphere (close to half of today's level) is determined based on the persistence of widespread anoxia in the ocean interior (Figure 2). Anoxia is determined principally here through the speciation of iron minerals in shales throughout the Proterozoic and Cambrian (Sperling et al., 2015), where deeper water samples show a dominance of highly reactive phases which are only found in such quantities in sediments overlain by anoxic water (Poulton and Canfield, 2005). The association of deep ocean anoxia with atmospheric O_2 levels less than ~12% atm. is based on simple box-modelling of the supply and demand of oxygen in the water column (e.g. Figure 1). The present-day O_2 supply exceeds the demand for respiration of sinking organic matter and thus the ocean interior is oxic, but this would not be the case if the mixed layer O_2 concentration were reduced by about half (Canfield, 1998; Watson et al., 2017). Recent 3D modelling work has shown that due to changing ocean circulation under different continental configurations, substantial parts of the deep ocean could have been anoxic in the early Paleozoic even under present-day atmospheric O_2 levels (Pohl et al., 2022). Nevertheless, the continental shelves, where the geochemical data supporting anoxia is found, tend to remain relatively well-oxygenated in these simulations. Further work with 3D models is required to better constrain atmospheric oxygen levels using marine geochemical records.

The lower limit for oxygen associated with the demands of Ediacaran and Cambrian biotas is also a useful benchmark for minimum O_2 levels, and sits at around 0.2% in the Ediacaran and around 2% in the Cambrian (Sperling, 2015). These were determined through an assessment of the O_2 demands of present-day sponges (as analogues to the Ediacaran biota; Mills et al., 2014) and Oxygen Minimum Zone (OMZ) seafloor animals (Levin, 2003). A much more certain lower limit exists from the mid-Silurian onwards and is defined by the presence of inertinite in sediments between 430–0 Ma. Inertinite is a by-product of wildfires which require high levels of oxygen to proliferate. Experiments have determined that fires cannot sustain themselves below 15% O_2, setting a clear lower limit for much of the Phanerozoic (Belcher and McElwain, 2008; Belcher et al., 2013; Glasspool and Gastaldo, 2022). There are periods after the charcoal record begins (e.g. during the Devonian, the early Triassic and the very early Cretaceous) when inertinite is sparsely recorded or absent, and it is uncertain if this is related to low pO_2 or unfavourable conditions for preservation (Diessel, 2010; Glasspool and Scott, 2010; Scott and Glasspool, 2006).

4. Methods of Phanerozoic O_2 estimation

We group the O_2 reconstruction methods into those that infer oxygen concentration in the atmosphere directly, those that rely on changes in marine redox to infer atmospheric O_2, and those that are based on broader aspects of Earth's global elemental cycles. These are shown in Figures 3a, 3b and 3c respectively. In this figure, O_2 reconstructions that are generally consistent with the long-term constraints from Section 3 are coloured in blue or green, whereas reconstructions which clearly violate the constraints are coloured in orange or yellow. Isotope Mass Balance (IMB) techniques will be discussed separately in Section 5.

4.1. Direct atmospheric methods for atmospheric O_2 reconstruction

The following methods are based on attempts to sample ancient air directly, or to record aspects of the terrestrial environment that are strongly linked to atmospheric oxygen, such as the prevalence of wildfires and the oxygen concentration in soils. These proxies have great potential for accurate reconstruction, but generally suffer from poor spatial coverage and time resolution.

4.1.1. Ice core records

The clearest way to estimate past levels of oxygen in the atmosphere are from ice core records, which contain samples of ancient air trapped in bubbles within the ice. This method has been famously used to determine ancient CO_2 levels over the Quaternary period (e.g. Petit and Raynaud, 2020), and current estimates of oxygen concentration from ice core samples indicate that pO_2 has declined from ~21.14% to ~20.95% of the atmosphere over the last 1.5 Myr (Extier et al., 2018; Stolper et al., 2016; Yan et al., 2019). This is shown as an inset in Figure 3a, as the relatively short time span is not easily visible when looking at the whole Phanerozoic. Ice core records are currently not available beyond about 2.7 Ma (Yan et al., 2019), thus despite their incredible fidelity, their usefulness in determining Phanerozoic-scale O_2 variations is limited.

4.1.2. Halite gas inclusions

Halite is a mineral that is formed when water evaporates. This process can result in fluid inclusions in the halite minerals, derived from the original body of water. Within those fluids it is possible to find bubbles of trapped air. A rigorous screening process has been developed to ensure that these fluid inclusions and gas bubbles have the best chance of

reflecting the atmospheric composition of the time (Blamey and Brand, 2019), and the Phanerozoic samples collected so far that meet these criteria (from Brand et al., 2021; Blamey et al., 2016) are shown in Figure 3a and coarsely span the Ordovician to Paleogene. Uncertainty was calculated by assessing concentrations of oxygen versus organic-matter-derived gases in the samples in order to estimate the original O_2 concentration before any reactions took place. This can generate a large uncertainty window, and in some cases samples of the same age have non-overlapping uncertainties (Figure 3a) (Brand et al., 2021) which may indicate problems with preserving original signals, or with the method used to 'back calculate' the original composition.

A potential problem with the method appears most clearly when looking at samples from the Archean, which indicate an atmospheric O_2 level of 3% atm. - one seventh of the present-day level (Steadman et al., 2020). This is vastly higher than the upper limit of one millionth of the present-day level (Figure 2) set by the Archean MIF-S record (Farquhar et al., 2000), and the similar upper limits set by the absence of iron oxides, the presence of detrital reduced minerals which would be oxidised at even low atmospheric O_2 (Holland, 2006; Kump et al., 2013; Rasmussen and Buick, 1999) and a lack of isotope fractionation in elemental cycles (Cr, Mo, U) that readily produce these signals in the presence of oxygen (see Catling and Zahnle, 2020). Thus, while the potential to sample ancient air makes this method appear very promising, this issue of major disagreement with the overwhelming majority of Archean O_2 estimates remains to be resolved.

4.1.3. The charcoal record

Fossil charcoal is an indicator that wildfires occurred in the geological past (Scott, 1989; Scott and Jones, 1991). Dead vegetation undergoes peatification and then coalification,

with the resultant coal composed of different groups of macerals, dependent on the method of breakdown (e.g. physical, chemical, bacterial). One maceral group: inertinite, of which fusinite (mostly fossil charcoal) belongs to, is formed primarily due to pyrolysis of vegetation by wildfires (Scott, 1989; Scott and Jones, 1991; Scott and Glasspool, 2007). As well as oxygen, wildfires require heat, fuel, and an ignition source, such as lightning strikes, which themselves can be identified in the fossil record (e.g. Cope and Chaloner, 1980; Pyne et al., 1996; Scott and Jones, 1991). The presence of inertinite in the geologic record indicates that there was sufficient oxygen in the atmosphere to sustain wildfires for much of the last ~430 Myr (Glasspool and Gastaldo, 2022), but there have also been attempts to use the fossil charcoal record to generate quantitative estimates of Phanerozoic pO_2. A database of the percentage by volume of inertinite in coals (Inert%, e.g. normalised to the volume of coal) was collated, binned into 10 Myr intervals, and used to calculate pO_2 by generating calibration curves and deriving a power law relationship (Glasspool and Scott, 2010). At 21% O_2 the mean Inert% is 4.3% (based on Pleistocene to Recent samples), and it was assumed that with an Inert% of 0.2% (equivalent to a single charcoal particle in a coal sample) this would equal the experimental minimum O_2 of 15% atm (Belcher and McElwain, 2008). A maximum abundance of inertinite occurs during the early Permian (280 Ma), where Inert% = 44.4% and this was assumed to correspond to a pO_2 level of 30% atm, beyond which it was predicted that fires would be so widespread as to limit any further oxygen rise through limitation of photosynthetic productivity. An update to the method, using S-shaped calibration curves instead, was applied to the Paleozoic by Glasspool et al. (2015). Here we use the updated method to re-calculate the Mesozoic and Cenozoic data from Glasspool and Scott (2010) and plot the results in Figure 3a. Overall, the charcoal curve describes a rise in O_2 levels during the Devonian, high levels in the Carboniferous-Permian, and a long decline between the Cretaceous and the present day.

4.1.4. Fossil plant root morphology

Plants require oxygen to perform aerobic respiration. Specifically, the roots must respire in order to take up nutrients, and for tissue maintenance and growth, thus setting a minimum oxygen concentration in the soil at the root depths. A new method (Sønderholm and Bjerrum, 2021) uses a soil-root model to calculate the drawdown of O_2 from the atmosphere to the soil, based on the known depth of plant roots in the past and the soil medium. This is then used to infer atmospheric O_2 levels. Currently this method has only been applied to *Archaeopteris*, an extinct link between the ferns and the gymnosperms (non-flowering, seed-producing plants) which lived during the Devonian and Carboniferous (Sønderholm and Bjerrum, 2021). The calculated O_2 required for optimal growth is around 17% atm, shown in Figure 3a. It is possible that *Archaeopteris* could have survived at ~12% O_2 as an absolute lower limit, but the evidence for wildfire suggests that O_2 levels were 15% or higher.

4.2. Atmospheric O_2 inferred from marine redox proxies.

Marine sediments are plentiful throughout the Phanerozoic, and a large number of proxy tools have been developed to infer the redox state of the overlying water column, or the global ocean, from either enrichments, distribution of an element between different species, or isotope fractionations. As detailed in Section 3, iron speciation has documented widespread anoxic seafloor conditions before the Ordovician (Sperling et al., 2015) which is used to infer an upper limit for atmospheric O_2 levels during this time. Some studies have sought to use marine redox proxies to make quantitative estimates of the changes in atmospheric O_2 levels throughout the Phanerozoic. All of these methods are in conflict with the lower limit set by the charcoal record, and we attribute this mismatch to the difficulty in extrapolating precise atmospheric O_2 levels from marine oxygenation. The ocean is a tiny reservoir of oxygen compared to the atmosphere, holding less than 1% of the surface O_2 budget. Also, marine redox

is highly spatially-variable and is controlled at the local scale by the availability of organic matter and O_2 consumption by respiration (see Figure 1). Finally, the preserved sediment record, particularly pre-Jurassic, is strongly biased towards shallow marine epicontinental seas, which have an unclear relationship to conditions in the wider ocean. Given these uncertainties and others, most marine redox proxies have not been converted into a quantitative estimate of atmospheric O_2 levels, but the few that have, are explored below and are plotted in Figure 3b.

4.2.1. Cerium anomalies in carbonate sediments

Cerium is a rare-earth element (REE), a group of metals with similar properties but with sufficient differences to make the ratio of one REE to another a useful metric. Specifically, Ce, unlike the other REEs can be removed from solution by oxidation. This means that calculating a Ce depletion relative to the other REEs in carbonate sediments (a negative Ce anomaly) can indicate the presence of oxygen in the water column. Ce anomalies have been used as a qualitative metric for late Neoproterozoic and Phanerozoic oxygenation (Wallace et al., 2017), while a quantitative method calculates atmospheric O_2 concentrations from the Ce anomaly by assuming that shallow-water carbonates precipitate in environments in equilibrium with the atmosphere, thus the concentration of Ce can be related to atmospheric O_2 (Liu et al., 2021). The concentration of Ce is then related to the Ce anomaly by assuming other REE concentrations did not change over time. Both qualitative and quantitative analyses show a broad shift towards greater Ce anomalies during the Devonian, but the quantitative method predicts O_2 levels as low as ~0.2%, in contradiction to the inertinite record, at the start of the Devonian. It should be noted that Liu et al. (2021) were mostly concerned with calculating these concentrations over the Precambrian, for which their order-of-magnitude approach is more appropriate.

4.2.2. Carbon to phosphorus ratios in black shales

Organic matter from marine primary producers tends to comprise carbon and phosphorus in the ratio 106:1 (Redfield, 1958). Some of this organic matter eventually sinks to the sediments (e.g. Figure 1) where much of it is oxidised by microbes, transforming the carbon to CO_2 and releasing the phosphorus. Because microbes often focus on P-rich compounds, P is preferentially released during this process, leaving the remaining organics P-depleted (Algeo and Ingall, 2007). Further redox-dependent processes can then occur in the sediment which may trap this newly-liberated phosphorus, affecting the overall C_{org}:$P_{reactive}$ measured in the sediments (i.e. the ratio of organic carbon to soluble P). In general, high C_{org}:$P_{reactive}$ indicates that P has been recycled back to the water column and low C_{org}:$P_{reactive}$ suggests that P has been retained in the sediments. P retention in sediments is a strong function of oxygen availability, as much of the P trapping occurs through the formation of iron oxyhydroxides (van Cappellen and Ingall, 1994). Thus, when considering organic-rich ('black') shales at the global scale, the degree of P trapping (tendency for a low C_{org}:$P_{reactive}$) may be related to the oxygenation of the oceans in general, which can be related to oxygen supply from surface waters equilibrated with the atmosphere. This was the approach of Algeo and Ingall (2007), who used records of C_{org}:P_{total} in sediments as a proxy for C_{org}:$P_{reactive}$, and scaled the resulting qualitative O_2 curve to ensure it did not violate the constraints imposed by the existence of fossil charcoal (Wildman et al., 2004). More recent work on wildfires and the charcoal record (Belcher and McElwain, 2008; Glasspool et al., 2015; Glasspool and Gastaldo, 2022) have subsequently meant that the predicted O_2 curve no longer satisfies these constraints.

4.2.3. Selenium to cobalt ratios in pyrite grains

Selenium (Se) is sourced through the oxidative weathering of sulfide minerals. Therefore, the marine Se concentration is expected to increase when atmospheric O_2 levels are greater. Conversely, cobalt (Co) concentrations are expected to decrease when the ocean is oxygenated due to adsorption onto iron oxyhydroxides. Large et al. (2019) proposed that marine Se and Co concentrations are reflected in the concentration of these elements in sedimentary pyrite – where Se can substitute for S, and Co can be incorporated into the crystalline structure. They derived a proxy for atmospheric oxygen by dividing Se concentration by Co concentration, and scaling this at points in the Neoproterozoic and Phanerozoic to atmospheric O_2 reconstructions from other methods. A recent revision of this parameterisation instead uses a power law to relate Se and Co concentrations to atmospheric O_2 (Cannell et al., 2022). Figure 3b shows the best guess curve of Large et al. (2019) for the Phanerozoic. This reconstruction is not consistent with the charcoal record as it records several dips to very low atmospheric O_2 at times where wildfire was abundant (Glasspool et al., 2015). The revised formulation is not plotted as it has only been produced for the Paleozoic, but it too falls below the wildfire minimum (Cannell et al., 2022). Sulfide weathering has a weakening dependence on oxygen concentration when oxygen levels are high, and may be more dependent on erosion rates (Daines et al., 2017) and the action of the biosphere (Kanzaki and Kump, 2018). This could help explain why these O_2 reconstructions record rising O_2 levels over the Cenozoic, when global erosion rates are increasing.

4.3. Atmospheric O_2 inferred from sedimentary abundances and isotope fractionations

These methods (Figure 3c) are based on the Earth's long-term carbon cycle, and seek to reconstruct variations in atmospheric O_2 either directly from the burial rates of organic carbon and pyrite (the long-term O_2 sources, see Section 2), or from the carbon isotopes of

organic material, which can be related to photosynthesis - which is sensitive to the atmospheric O_2 : CO_2 ratio.

4.3.1. Sedimentary carbon and sulfur masses

Given that the total flux of O_2 production over geological time is related to the combined burial of organic carbon and pyrite, a simple but effective way to estimate the accumulation of O_2 in the atmosphere is to record the mass of these species in sediments around the world over the Phanerozoic. Berner and Canfield (1989) set out to do this by using existing global sediment records and their average C and S compositions to determine organic carbon and pyrite burial rates through time (Budyko et al., 1987; Ronov, 1976). Pyrite burial rates were constrained by adding an oxygen dependency, as the record of marine sediments did not include redox information. More pyrite burial is expected in anoxic and sulfide-rich conditions which are more prevalent at low O_2. This increases O_2 production and thus net pyrite burial starts to decrease, resulting in a strong negative feedback on O_2 levels from the S cycle. Consumption fluxes, through the weathering of organic carbon and pyrite, were also computed, and were based on sediment accumulation rates. The resulting atmospheric O_2 prediction has a large uncertainty, as one might expect given the generalised nature of the method. Nevertheless, the curve is consistent with the long-term constraints, although they suggest the very minimum of the uncertainty window should be taken during the Cambrian. The strong negative feedback from the S cycle may be why the ‘best guess’ model does not predict < 15% O_2 at any point in the Phanerozoic.

4.3.2. Carbon isotopes in plant resins

Photosynthesis converts carbon dioxide and water into oxygen and organic carbon. However, the reaction can also proceed in the opposite direction and consume oxygen – photorespiration – and the ambient O_2 concentration is a major factor in determining how efficient photosynthesis is. Tappert et al. (2013) used fossil plant resins (e.g. amber) as a $\delta^{13}C$ archive of plant materials over time to estimate changes in atmospheric O_2 based on this photosynthetic efficiency. They opted to use a direct proportionality between isotopic fractionation and O_2 levels, rather than a laboratory-measured curve for isotopic fractionation at different O_2 levels (Berner et al., 2000), because the degree of fractionation was much smaller than Berner et al. (2000) obtained. Their reconstructed O_2 curve falls well below the wildfire limit for much of the Mesozoic. This may be due to uncertainties in what is controlling plant resin $\delta^{13}C$ values, given that precipitation can impart differences of up to up to 6‰ (Diefendorf et al., 2012), similar to the measured range in Tappert et al. (2013), and might explain smaller fractionation in the Mesozoic where precipitation was restricted on the supercontinent Pangaea (e.g. Otto-Bliesner, 1995).

4.3.3. Measuring photosynthetic response to O_2 levels

Changes in photosynthetic efficiency, as discussed in Section 4.3.2. also impact the isotopic composition of the organic carbon created. Laboratory experiments have determined relationships between O_2 levels and the isotopic fractionation (i.e. change in isotopic composition) imparted by photosynthesis (Beerling et al., 2002; Berner et al., 2000). Therefore, the isotopic composition of carbon in the geological record can be used to estimate O_2 levels. Edwards et al. (2017) used paired isotope values from organic and inorganic carbon in Ordovician sediments to estimate this photosynthetic effect directly, and therefore make a

prediction for atmospheric O_2 levels. Their results indicate a rise in O_2 levels which is consistent with the long-term constraints.

4.4. O_2 reconstructions using isotope mass balance

Isotope Mass Balance (IMB) is a technique that aims to reconstruct the global O_2 source from sedimentary isotope ratios, rather than from rock masses. The advantage over the rock mass method is that isotopic information is available in high fidelity throughout Phanerozoic time, and is not clearly influenced by the poor preservation of more ancient sediments, or changing average compositions of sediment types. The method hinges on the isotopic discrimination imparted by photosynthesis, which leaves the $\delta^{13}C$ value of organic carbon around 27‰ lighter than the CO_2 – or marine bicarbonate – from which it is derived, although many factors, including O_2 levels as mentioned previously, can alter this (Berner et al., 2000; Beerling et al., 2002). With knowledge of the isotopic composition of the global inorganic carbon reservoir (recorded in carbonate rocks), and of the isotopic composition of global carbon inputs (i.e. volcanic CO_2) it is possible to calculate the fraction of total carbon burial that was organic. Knowing that total carbon burial must equal the total carbon input over long timescales, the organic carbon burial rate, and net production of O_2 can be calculated.

$$BC_{org} = BC_{total} \times (\delta^{13}C_{carb} - \delta^{13}C_{input}) / \Delta C \qquad (1)$$

Where BC_{org} is the global organic carbon burial rate, BC_{total} is the total (organic plus inorganic) carbon burial rate, $\delta^{13}C_{carb}$ is the carbon isotopic composition of carbonate rocks, $\delta^{13}C_{input}$ is the average carbon isotopic composition of volcanic CO_2 and all carbon weathering, and ΔC is the photosynthetic fractionation factor (around -27 ‰).

This IMB approach was first derived by Garrels and Lerman (1984) and then employed in several papers by Berner (1987, 2001), ultimately forming the basis of the GEOCARBSULF

model for atmospheric O_2 over Phanerozoic time (Berner, 2006). In these papers a sulfur cycle IMB was also employed alongside the carbon IMB shown above, in order to calculate pyrite burial rates. The sulfur cycle has a similar isotope discriminating process – sulfate reduction – which makes buried pyrite around 35‰ lighter than the seawater sulfate from which it was derived.

$$BS_{pyr} = BS_{total} \times (\delta^{34}S_{sw} - \delta^{34}S_{input}) / \Delta S \quad (2)$$

where BS_{pyr} is the global pyrite burial rate, BS_{total} is the total (pyrite plus gypsum) sulfur burial rate, $\delta^{34}S_{sw}$ is the sulfur isotopic composition of seawater (reflected in the composition of sulfate minerals), $\delta^{34}S_{input}$ is the average sulfur isotopic composition of both volcanic and weathering derived sulfur, and ΔS is the sulfate reduction fractionation factor (around -35‰).

Both the carbon and sulfur cycles employed in the GEOCARBSULF model are shown in Figure 4a. Because the total rates of carbon and sulfur input into the atmosphere and oceans are required to calculate the O_2 source, and because processes that consume O_2 must also be considered, the model is run forwards in time. The model is subject to an assumed global CO_2 degassing rate, and calculates surface processes like continental weathering in response to global temperature change. It estimates the isotopic composition of each reservoir, the input and output fluxes, and the amount of O_2 and CO_2 in the atmosphere and ocean at each timestep in accordance with the modelled processes. For a more detailed review of GEOCARBSULF see Berner (2006), Royer et al. (2014) and Mills et al. (2019).

Figure 4b shows the Phanerozoic O_2 predictions from recent versions of the GEOCARBSULF model. Royer et al. (2014, black line) updated Berner's original methodology with new estimates for continental weathering, and their results are similar to the O_2 trends that the model has produced since the initial 2006 version. The model has always

predicted near present-day oxygen levels in the early Paleozoic, a Permo-Carboniferous maximum, and a dip to low values either close to or below the fire minimum at around 200–150 Ma (Belcher and McElwain, 2008; Berner, 2009). These O_2 predictions show some clear similarities to the carbonate $\delta^{13}C$ and sulfate $\delta^{34}S$ records which were used to drive the model. In general theory, higher $\delta^{13}C$ values in carbonates reflect heavier seawater values, which can be a product of higher rates of photosynthesis and carbon burial removing the lighter isotope. Similarly, higher sulfate $\delta^{34}S$ values are generally interpreted as higher rates of pyrite burial, which also denotes a net source of O_2. The IMB equations shown above are consistent with these statements, but the calculated O_2 flux may also be altered if, for example, the isotopic composition of carbon or sulfur inputs were to change.

While Royer et al. (2014) had updated the $\delta^{34}S$ record to use data compiled by Wu et al. (2010), it was not until 2018, almost a decade after Berner's final contribution, that the $\delta^{13}C$ input data was revised (Schachat et al., 2018, red dashed line). This update changed the model predictions substantially, raising O_2 levels clearly above the fire minimum in the Mesozoic, and removing the prominent Permo-Carboniferous maximum. This modification also substantially increased the predicted oxygen concentration in the early Paleozoic, to above 35% during the Cambrian, which is difficult to reconcile with a long-term persistence of marine anoxia (Sperling et al., 2015). Contradictory behaviour like this in the early Paleozoic spurred an investigation into the processes responsible, which led to the model revision by Krause et al. (2018, blue line).

As discussed above, $\delta^{13}C$ fractionation during photosynthesis is dependent on atmospheric O_2 concentrations, with greater fractionation occurring at higher O_2 levels.

Practically, this means that as O_2 increases in the model, ΔC increases in equation 1, and the burial rate of organic carbon calculated to satisfy the isotope record decreases. Berner (2001) added a similar but much stronger effect to pyrite burial in the model, with $\delta^{34}S$ fractionation also dependent on atmospheric O_2. This was based on observations for increased fractionation when sulfide reoxidation was a major component of the sulfur cycle (Canfield and Teske, 1996). However, both the relationship of reoxidation to O_2 levels, and the necessity for this process to drive large isotopic fractionations, are uncertain (Jørgensen and Nelson, 2004; Krause et al., 2018; Sim et al., 2011). The strength of the feedback function applied in GEOCARBSULF was such that an atmospheric O_2 mixing ratio of 2.5% (i.e. the minimum required for the Cambrian biota) would result in a $\delta^{34}S$ fractionation factor of around 4‰, far below anything recorded during the Phanerozoic, and implying a massive rate of pyrite burial and net O_2 production in order to fit the isotopic data.

Krause et al. (2018) removed the IMB for pyrite burial and replaced it with a 'forwards' method, calculating pyrite burial rates from the availability of organic matter, sulfate, and oxygen. Instead of using the geological sulfur isotope record as an input, the model could predict the $\delta^{34}S$ of sulfates and this was compared with the geological record (Krause et al., 2018). This version of the model was renamed GEOCARBSULFOR – reflecting the 'forwards' sulfur cycle – and while the Mesozoic and Cenozoic results were similar to Schachat et al. (2018), the early Paleozoic O_2 levels were considerably lower, in line with the long-term O_2 constraints. Because of the highly-detailed carbonate $\delta^{13}C$ record, IMB is able to produce the highest resolution O_2 reconstructions of any method available. Nevertheless, the method relies on a series of important assumptions and datasets, and still has high uncertainty.

4.5 Forwards models of atmospheric O_2

A forwards (or predictive) model is one in which only the most basic tectonic and evolutionary boundary conditions are defined from the geological record, and the model attempts to predict from there the evolution of the Earth system using process-based descriptions of global biogeochemistry and climate (e.g. COPSE: Bergman et al., 2004; Lenton et al., 2018; MAGiC; Arvidson et al., 2013; SCION: Mills et al., 2021). Here, oxygen production is controlled directly by biological productivity and carbon burial, which is dependent on the liberation of nutrients through continental weathering. These models produce predictions of Phanerozoic atmospheric O_2 levels. However, the purpose of these models is to understand what drives changes in the Earth system and their predictions were never intended to be used as 'best guess' scenarios for atmospheric O_2. Thus, we do not include the results of these models in this attempt to establish consensus over atmospheric O_2 evolution.

5. Towards a consensus curve for Phanerozoic atmospheric O_2

We now try to best combine what we know about atmospheric O_2 variation over Phanerozoic time into a single curve and uncertainty window. We believe such a curve is needed due to a rapid expansion in available methods to reconstruct O_2 (see Section 4), combined with a tendency in the literature to plot forwards model outputs (Arvidson et al., 2013; Lenton et al., 2018), obsolete model versions (Bergman et al., 2004; Berner 2006) or even studies which test the limits of models (Zhang et al., 2018) in place of genuine O_2 reconstructions. This section will introduce our first attempt at this curve. Because of the very high time resolution possible, and the lack of any clear disagreement with the long-term constraints, we will use the IMB O_2 predictions as the central line in this curve, but will expand the uncertainty window to cover all of the current methods which themselves do not violate the

long-term constraints. In this way a ‘best guess’ for both short and long-term O_2 variations can be made.

5.1. Update to the Isotope Mass Balance approach

Because IMB depends on the $\delta^{13}C$ record, as well as (for example) reconstructions for tectonic CO_2 degassing rates, it is necessary to update these input parameters when new data becomes available. We do this within the GEOCARBSULFOR model, rather than GEOCARBSULF, due to the aforementioned uncertainty and violation of the long-term constraints on O_2 from the sulfur cycle in the original GEOCARBSULF (Krause et al., 2018). We have updated GEOCARBSULFOR further here by running Monte Carlo simulations to produce an envelope of uncertainty (as in Royer et al., 2014). We vary five key variables which have a high degree of control over predicted O_2 levels: uncertainty in the long-term records of $\delta^{13}C_{carb}$; tectonic degassing; continental erosion; the assumed climate sensitivity to changes in CO_2 levels; and the scaling coefficient which links changes in photosynthetic $\delta^{13}C$ fractionation to atmospheric O_2. For these five variables we sample equally between maximum and minimum bounds, running the model 5,000 times by utilising MATLAB’s parallel computing toolbox. Code to perform single runs of the model, and the Monte-Carlo procedure, is freely available (at https://github.com/Alexjkrause). This webpage also includes the model equations, which can also be found in Krause et al. (2018). The present model updates are detailed below.

5.1.1. The $\delta^{13}C_{carb}$ record

The $\delta^{13}C_{carb}$ record is used to infer the $\delta^{13}C$ composition of seawater across the Phanerozoic, and is employed to calculate the organic carbon burial flux through IMB. In the previous version of GEOCARBSULFOR (Krause et al., 2018; hereafter GEOCARBSULFOR-

2018), this was based on the compilation by Saltzman and Thomas (2012). The data from 540 Ma to present was placed into 5 Myr bins and a 10 Myr moving average was applied to generate an average record. The $\delta^{13}C$ value at 540 Ma was used for the model spin-up phase (570 – 540 Ma). For our update, we now use the compilation of Cramer and Jarvis (2020). We place the data from 538.8 – 0 Ma into 2 Myr bins and calculate an average and ± 1σ as the uncertainty range for the Monte-Carlo ensemble (Figure 5a).

The higher fidelity of the new record, and our smaller bins, allow the model input curve to faithfully represent the variations in $\delta^{13}C_{carb}$ on the ~million year timescale. This record is assumed by the model to represent the average carbon isotope composition of the ocean, but this is not completely straightforward as the Paleozoic record is almost entirely from epicontinental (inland) seas, due to the subduction of most records deposited in deeper waters. Such environments can develop $\delta^{13}C$ values around 1‰, or perhaps a maximum of 2‰ higher than the ocean mean. The record we use here was constructed based on the principle that it should reflect mean ocean values, ensuring there was no clear step-change in the isotope record when it switched to records from deeper settings (Cramer and Jarvis, 2020).

5.1.2. Tectonic degassing

Normalised degassing rates were used in GEOCARBSULFOR-2018 to help generate estimates of carbon or sulfur emissions to the ocean-atmosphere system from the combination of tectonism and metamorphism. These were based on seafloor spreading, as a general approximation to degassing at both mid-ocean ridges and subduction zones. The rates for 0 to 150 Ma were calculated by using data from Engebretson et al. (1992), and earlier rates were based on the sea-level record, which was ‘inverted’ to produce ridge volumes and thus degassing rates (Gaffin, 1987). Since then, improved estimates of degassing have been made

through full-plate modelling (Domeier and Torsvik, 2017) and compilations of the extent of volcanic arcs (Mills et al., 2017) and rifts (Brune et al., 2017). In the revised model we take the degassing rate uncertainty range from Mills et al. (2021), which is bounded by reconstructions of arc and rift lengths, and by estimates from full plate models.

5.1.3. Uplift and erosion

Previously, the formulation for the uplift and subsequent erosion of sediments (which affects chemical weathering) was based on a polynomial fit to the depositional record of terrigenous sediments (Berner and Kothavala, 2001; Ronov, 1993), assuming that erosion rates over the Phanerozoic can be calculated from deposition rates using an erosion-loss relationship (Wold and Hay, 1990). The data were normalised to the erosion rates for the Miocene, rather than the Pliocene or Quaternary, in order to avoid the effect of extensive continental glaciation over the last ~5 Myr on the observed rate (Berner and Kothavala, 2001). Erosion was assumed to affect silicate, organic carbon and sulfide weathering, but not carbonate or sulfate weathering, as it seemed that elevation had little effect on carbonates and sulfates, which can readily dissolve in the subsurface (Berner, 1991, 2006; Berner and Berner, 1987).

Using the sediment abundance data of Hay et al. (2006), we create minimum and maximum bounds for the Monte Carlo runs by normalising the data to that of the Pleistocene and Miocene, respectively, and then employ a 100 Myr moving average. Following Li and Elderfield (2013), we include the effect of erosion in the equation for carbonate weathering and assign it a near-linear relationship, while erosion in silicate, organic carbon and sulfide weathering holds a weaker association.

5.1.4. Effect of O_2 levels of carbon isotope fractionation

As discussed in Section 4, an equation based on plant and algal growth experiments (Beerling et al., 2002; Berner et al., 2000) was used to calculate the changes to photosynthetic $\delta^{13}C$ fractionation at different O_2 levels. The equation required the use of an empirical coefficient, named *J*, which was set to be equal to 4 and seemed to produce $\delta^{13}C$ fractionation in line with that from an even mixture of marine and terrestrial organic matter through time (Beerling et al., 2002; Berner, 2009; Hayes et al., 1999). Edwards et al. (2017) used different values for *J* and showed that, in their formulations at least, this parameter had a significant effect on the estimated O_2 levels; while sensitivity testing of this parameter in GEOCARBSULFOR (Krause et al., 2018) exhibited a far more muted effect, possibly due to other feedbacks in operation. Nevertheless, we include this parameter in the Monte Carlo runs, with minimum and maximum bounds of 2.5 and 7.5, respectively, following Edwards et al. (2017).

5.1.5. Climate sensitivity

The long-term climate sensitivity – the global temperature change expected per CO_2 doubling – is important in estimating the rates of continental weathering through time. In GEOCARBSULF, the climate sensitivity changed through the model run, such that it was approximately 4.32 K per CO_2 doubling during 'greenhouse' periods (e.g. the Cretaceous) and approximately 8.66 K during 'icehouse' periods (e.g. the Carboniferous). We instead add climate sensitivity to our Monte-Carlo parameters, using the bounds of 4 K and 6 K per CO_2 doubling, which encapsulates the expected Phanerozoic range (e.g. Mills et al., 2019; Royer et al., 2016).

5.1.6. Model stability at low O_2

The GEOCARBSULF and GEOCARBSULFOR models are highly sensitive to the $\delta^{13}C$ record used as a model input, and very low $\delta^{13}C$ values can result in model failure when more than the entire reservoir of atmospheric and marine O_2 is consumed in a single time step. This problem prevented complete sensitivity analysis being performed by Royer et al. (2014) and Krause et al. (2018). In the updated model we use a logistic function to turn off all O_2-consuming fluxes when oxygen concentration falls below 0.02% atm. or 1000 times less than the present day, which prevents over-depletion of the oxygen reservoir and stops the model crashing during the runs. We still find about 5% of the Monte-Carlo runs crash during the model 'spin-up' phase from 570–539 Ma where reservoirs initially change size much more rapidly than during the Phanerozoic as the model is adjusting to the starting conditions.

5.1.7. Updated Phanerozoic O_2 reconstruction

New predictions from GEOCARBSULFOR are shown in Figure 5b and 5c. Firstly, the $\delta^{34}S$ record is compared to compiled geological data to ensure that the forwards-calculated sulfur cycle in the model is reasonable. As in Krause et al. (2018), these predictions are in reasonable agreement with the geological record (Crockford et al., 2019). The long-term pattern of Phanerozoic atmospheric O_2 evolution is similar to the previous iteration of the model (Krause et al., 2018), but the new higher fidelity $\delta^{13}C$ record results in more variability in O_2, particularly during the early Paleozoic, with more cyclicity during the Cambrian through to the Devonian. O_2 levels are low during the early Paleozoic, and are generally beneath the threshold indicated by widespread ocean anoxia (Canfield, 2014; Sperling et al., 2015). The model mean dips slightly below the wildfire minimum during the Devonian but the uncertainty window remains above the limit. The overall O_2 maximum is shifted back to the Permian, in

line with the older GEOCARBSULF models (Berner, 2006, 2009). There is also a more pronounced decline in O_2 levels from the end of the Permian across the Triassic.

5.2. A best guess for changes in O_2 across the Phanerozoic

Figure 6 shows our new combined estimate for Phanerozoic O_2 evolution. The best guess line is the same as that calculated for Figure 5c from IMB and the uncertainty window is produced from a smoothed record of the local maximum and minimum from those methods described in Section 4 which do not violate the long-term oxygen constraints. Where parts of their uncertainty windows do violate the constraints, they have been trimmed accordingly. Many of these uncertainty windows overlap with the Monte-Carlo uncertainty from the IMB curve, and tend to place it close to the middle of the range. Exceptions to this are during the Ordovician, where the direct isotope fractionation method of Edwards et al. (2017) produces significantly higher O_2 (although with a similar trend), and during the Triassic–Jurassic where the minima from the charcoal inversion and the sedimentary rock mass methods point to lower O_2.

6. How do changes in O_2 relate to biological events?

Alongside our new Phanerozoic O_2 reconstruction in Figure 6 we plot a selection of key biotic events, consisting both of evolutionary radiations and crises. Firstly, the Cambrian Explosion occurred from roughly 541 – 514 Ma (Erwin et al., 2011; Maloof et al., 2010) and saw rapid diversification of all major animal phyla. Our O_2 reconstruction shows substantial variation in oxygen levels during this time, including a series of O_2 pulses during Cambrian stages 2 and 3 which have previously been linked to pulses of biodiversity (He et al., 2019). Without well-defined modelling of the preceding Neoproterozoic Era we cannot assess whether

679 the Cambrian explosion was triggered by rising O_2 levels, but the periodic changes in
680 biodiversity may well be linked to pulsed atmospheric oxygenation, which would translate to
681 changes in habitable space for animals on the continental shelves. A further expansion of
682 marine animal diversity occurred during the Great Ordovician Biodiversification Event
683 (GOBE), which spans the whole Ordovician period, concentrated in the Middle and Upper
684 Ordovician (Edwards, 2019; Servais and Harper, 2018). As in the reconstruction of Edwards
685 et al. (2017), we conclude that the Ordovician period was primarily a time of rising oxygen
686 levels, which may have been linked to this event. The Devonian saw a number of revolutions
687 in the diversity of fish in the oceans, including the evolution of large predatory fish, with their
688 higher O_2 demands (Dahl et al., 2010; Dahl and Hammarlund, 2011). The start of this Devonian
689 'Age of Fishes' may be extended back into the Silurian, when considering the increase in the
690 biovolume of Chordata (Payne et al., 2009) and a possible evolutionary split between the
691 lungfish and tetrapods (Zhao et al., 2021). It has been estimated that predatory fish need >7.4
692 – 11.7% O_2 (Dahl and Hammarlund, 2011), and our oxygen reconstruction suggests that this
693 threshold was indeed crossed by the late Silurian.

694 The Permian-Triassic Mass Extinction was the most severe of all the Phanerozoic mass
695 extinctions, with 55.7% genus extinction (Bambach, 2006; Benton and Twitchett, 2003; Erwin,
696 1993). According to our reconstruction, the PTME occurred at a time when atmospheric O_2
697 levels were the highest they have ever been, and considering the devastation and reduction in
698 biomass of terrestrial ecosystems during the event, and into the middle Triassic (Xu et al., 2022;
699 Chu et al., 2020; Dal Corso et al., 2020; Fielding et al., 2019), the extinction may have been a
700 driver of the subsequent long-term decline in O_2. In our reconstruction, O_2 levels eventually
701 stabilized at around 25% by the late Triassic, coincident with the evolution of mammals (Sulej
702 et al., 2020). The later evolution of large placental mammals in the early Cenozoic occurs after
703 a long period of gradually rising O_2 levels in our reconstruction (Falkowski et al., 2005), but is

also accompanied by a decline towards present-day levels, making it difficult to link to changes in oxygen concentration.

Overall, pulsed rises in atmospheric oxygen levels appear to be consistent with the Cambrian Explosion, GOBE, and rise of predatory fish, and the general trend throughout the Paleozoic is towards higher and higher atmospheric O_2 levels. This is consistent with a plant evolutionary driver given the successive floral changes occurring during the Paleozoic (Algeo et al., 1995) and the ability of larger and more productive plants to produce more oxygen, although these advances are generally poorly dated, especially in terms of when species rose to ecological dominance. A decline in atmospheric O_2 following the PTME is also consistent with widespread vegetation loss and delayed recovery, which was likely exacerbated by the aridity of the Pangea supercontinent, potentially limiting photosynthetic productivity on land until continental breakup from the Jurassic onwards (Chaboureau et al., 2014; Gurung et al., 2022). The drop in O_2 levels between the late Cretaceous and present day may be related to a decline in global temperatures and runoff over the same timeframe, both of which might be related to decreasing rates of CO_2 degassing (e.g. Brune et al., 2017; Domeier and Torsvik, 2017), which would decrease global temperatures and limit the terrestrial biosphere through low CO_2.

7. Conclusions

New methods for estimating Phanerozoic atmospheric O_2 evolution are widespread, and many older methods are being revised and revisited. At first look, it can be tempting to conclude that no consensus exists on Phanerozoic O_2. We have taken a critical look at the currently available methods and aimed to determine which are the most reliable by comparing them to broadly-agreed long-term constraints on oxygen concentration. Those methods which

currently fail this test are also subject to clear uncertainties in the methodology, which we have highlighted as potential reasons for the divergent results. We have then produced a first attempt at a consensus O_2 curve for the Phanerozoic by bringing together all of the methods which satisfy the long-term constraints. This curve shows that the Cambrian Explosion and Great Ordovician Biodiversification Event may well be linked to pulses of long-term atmospheric oxygenation, whereas the Devonian 'Age of the Fishes' appears to coincide with O_2 levels stabilising above the threshold which can maintain an oxic ocean interior.

Figures with captions

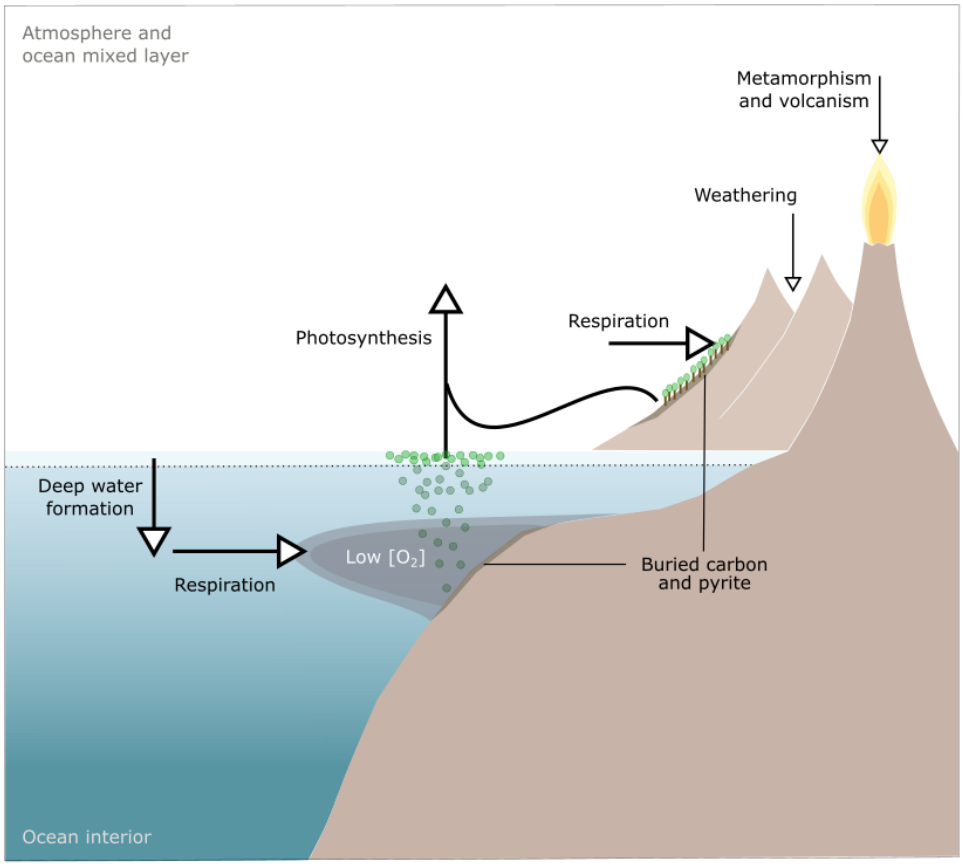

Figure 1. The global oxygen cycle. *The short term cycle of photosynthesis and respiration involves large fluxes but ultimately produces a small net source of O_2 proportional to the amount of buried carbon and pyrite. The long-term cycle balances this net source with the weathering and metamorphism of these carbon and pyrite-containing sediments.*

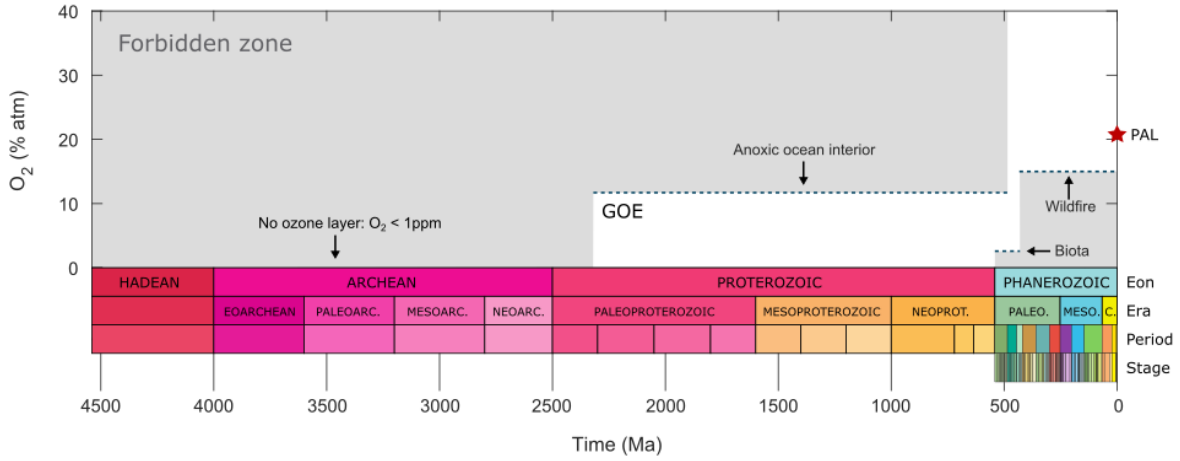

742

743 ***Figure 2. Long-term constraints on atmospheric O_2 over Earth history.*** *Upper limits are set*

744 *by the mass-independent fractionation of sulfur before ~2400 Ma, and by broadly anoxic*

745 *bottom waters until the Ordovician. Lower limits are set by the requirements of the animal*

746 *biota in the early Paleozoic, then by the existence wildfires from ~430 Ma to present. See text*

747 *for details of these limits. GOE = Great Oxidation Event. PAL = Present Atmospheric Level.*

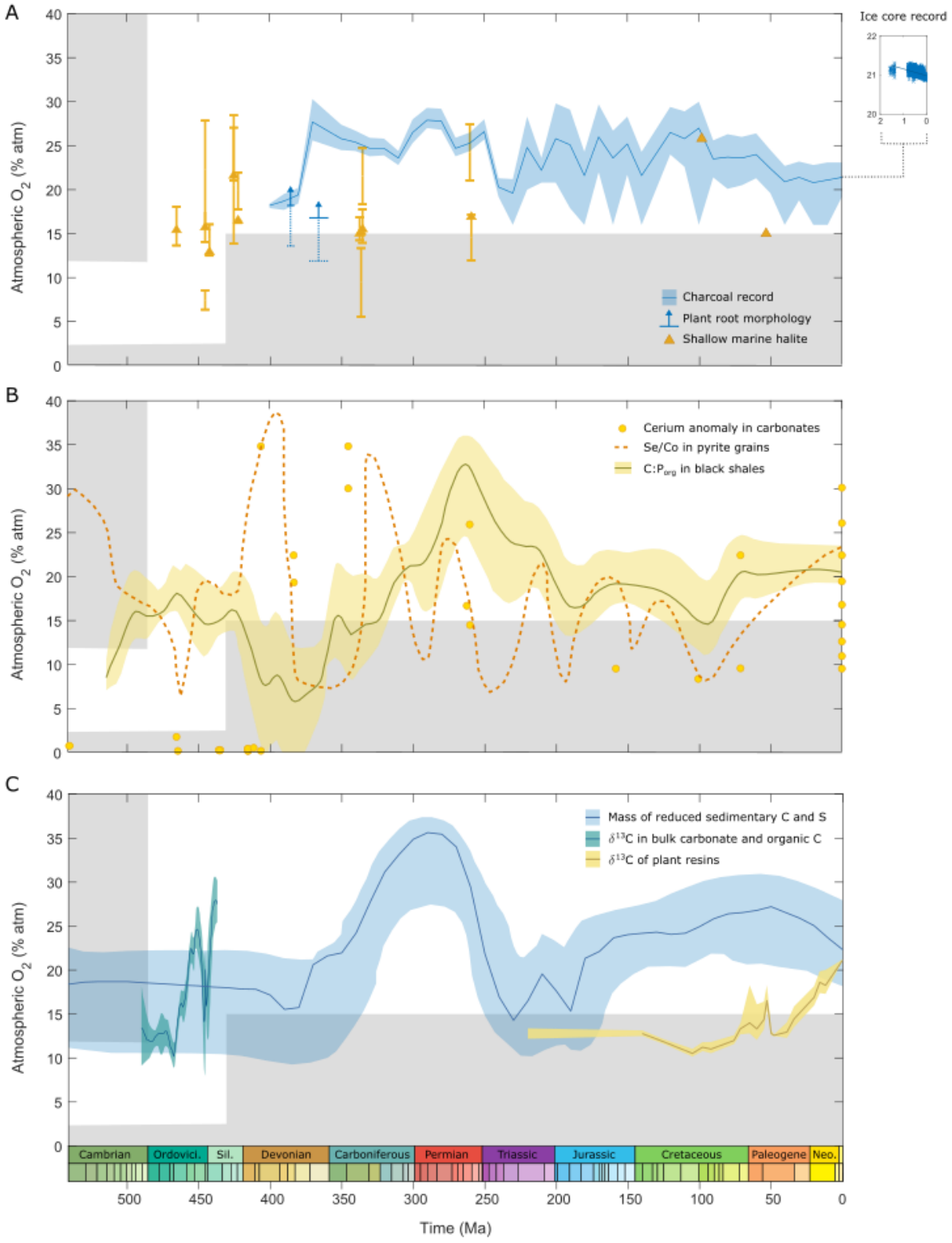

748

749 ***Figure 3. Phanerozoic O_2 estimates from geological and geochemical proxies***. *A. Direct*

750 *proxies for atmospheric composition (Section 4.1). B. Proxies related to marine oxygenation*

751 *related to atmospheric O_2 (Section 4.2). C. Sediment abundance and isotopic fractionation*

methods (Section 4.3). Blue/green colours denote estimates which will form part of our combined estimate, yellow/orange colours denote estimates which will not. See the listed text sections for further details and discussion of these methods. Grey areas show forbidden zone from Figure 2.

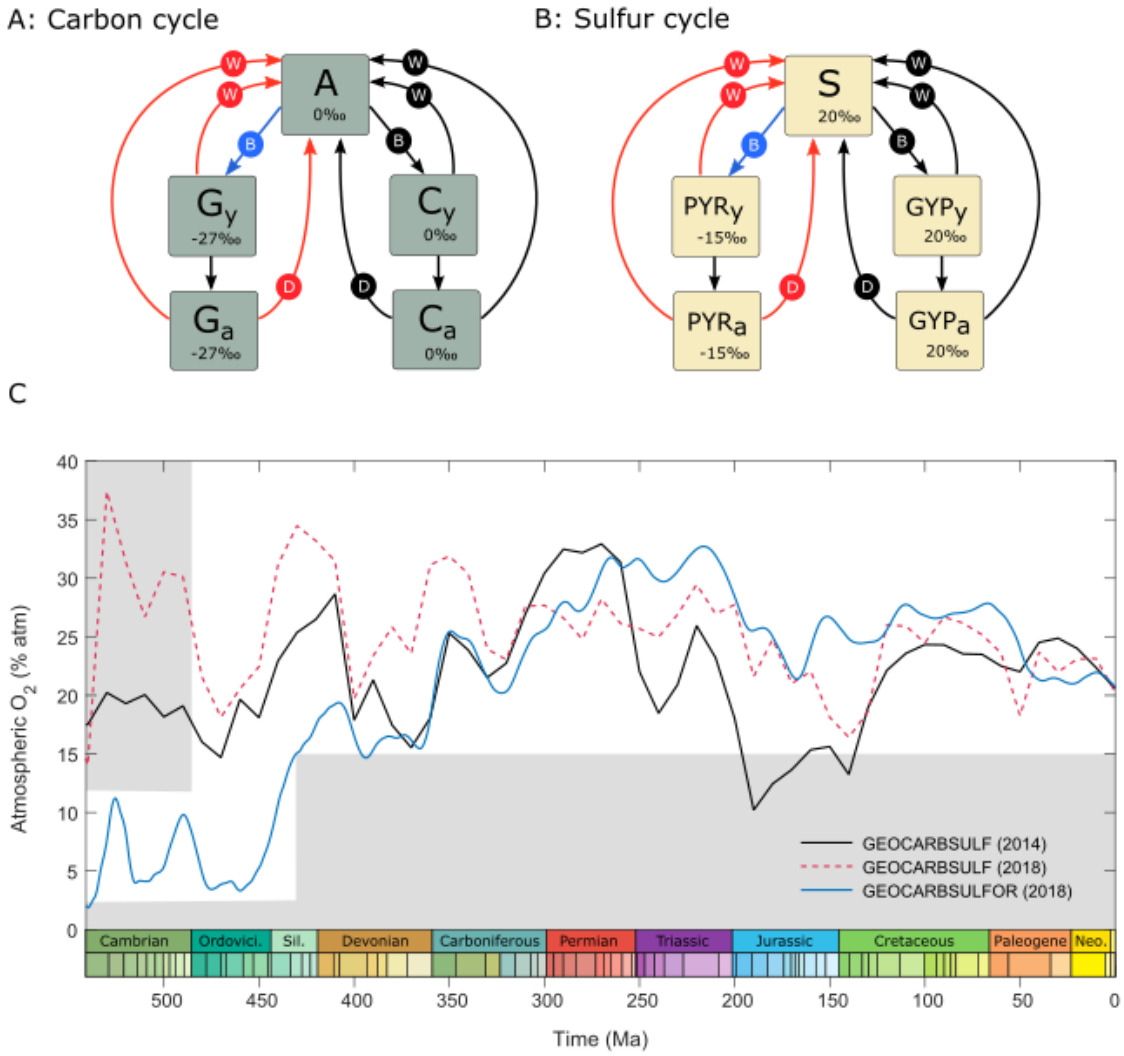

Figure 4. Isotope Mass Balance (IMB) techniques. *A. Schematic of the long-term carbon cycle as used in IMB modelling. Here W = weathering, B = burial and D = degassing. B. Schematic of the long-term sulfur cycle as used in IMB modelling. A = atmosphere and ocean carbon, Gy = young organic carbon, Ga = ancient organic carbon, Cy = young carbonates, Ca = ancient carbonates, S = ocean sulfate, PYRy = young pyrite, PYRa = ancient pyrite, GYPy = young gypsum, GYPa = ancient gypsum. C. Atmospheric O_2 predictions from IMB*

models. Black line shows GEOCARBSULF model of Royer et al. (2014). Red dashed line shows update using a more recent carbon isotope record to drive the model (Schachat et al., 2018). Blue line shows the same newer carbon isotope record plus an update to the model structure as in Krause et al. (2018). Se text for further details. Grey areas show forbidden zone from Figure 2.

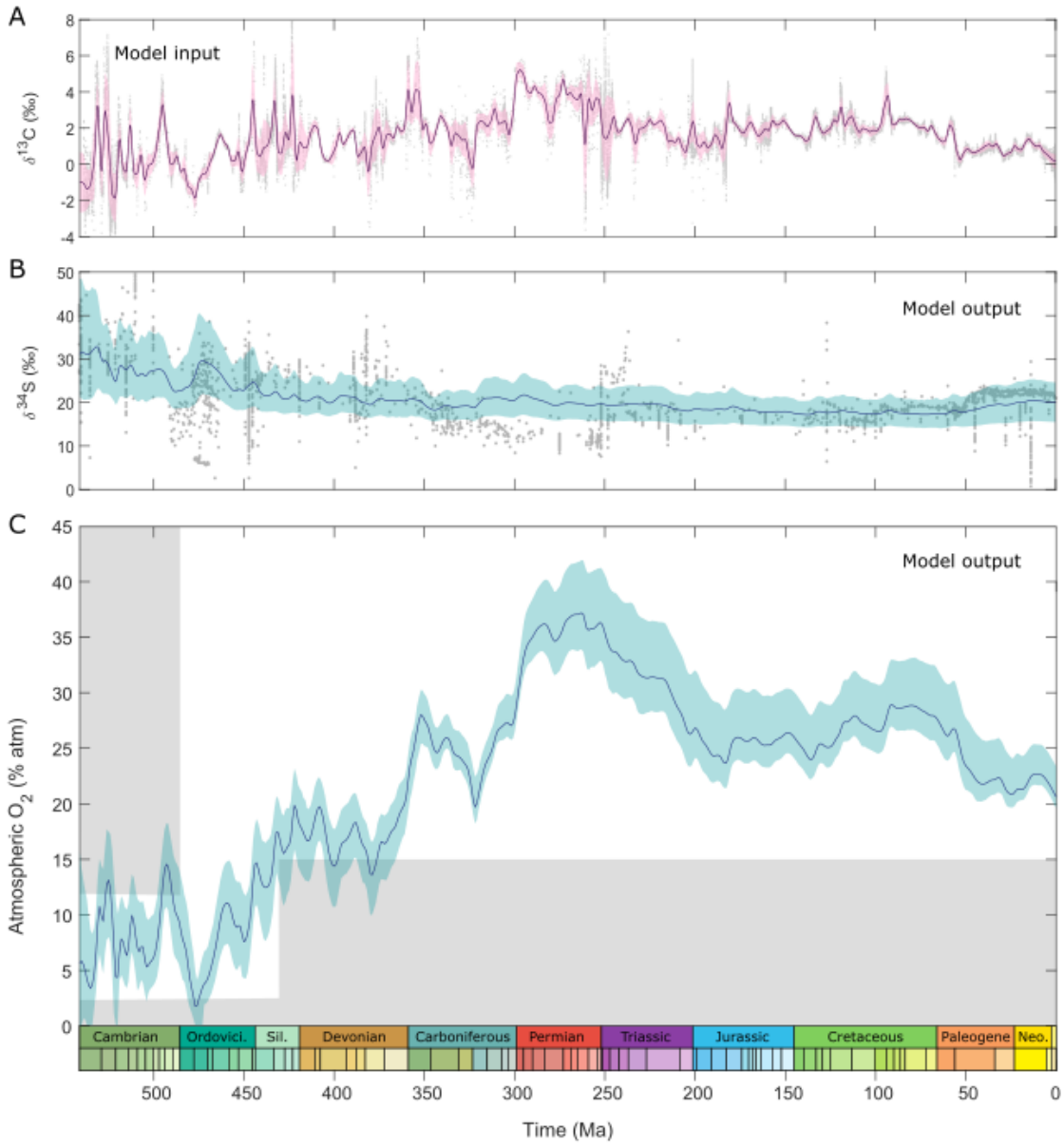

Figure 5. Updated Phanerozoic O_2 predictions from GEOCARBSULFOR. *A. Carbonate $\delta^{13}C$ record used as model input, from the GTS2020 (Cramer and Jarvis, 2020). B. Sulfate $\delta^{34}S$ record outputted by the model for validation, tested against the compilation of Crockford et al.*

(2019). C. Predicted Phanerozoic atmospheric O_2 evolution. Central line shows median and blue area shows full range of Monte-Carlo ensemble. See text for details of model and ensemble procedure. Grey areas show forbidden zone from Figure 2.

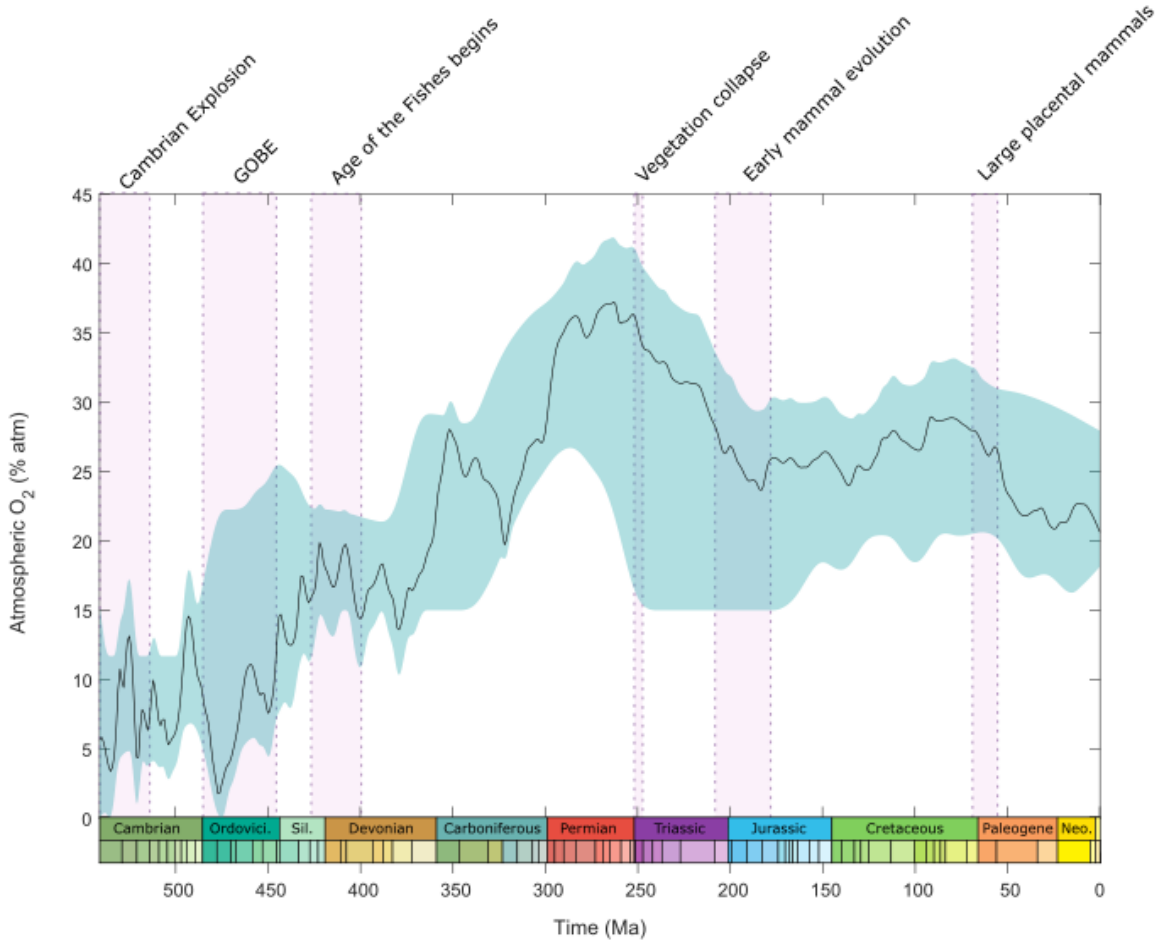

Figure 6. Towards a Phanerozoic O_2 consensus curve. *Blue shaded area incorporates all Phanerozoic O_2 estimations from Figure 3 which do not violate the long-term constraints shown in Figure 2. Uncertainty ranges have been trimmed as to not violate those constraints either. Superimposed on this are the new Isotope Mass Balance O_2 predictions from GEOCARBSULFOR, which also provide the central line. The O_2 variations are compared to key biological events. See text for further details.*

References

Ahm A-SC, Bjerrum CJ, Hammarlund EU. 2017. Disentangling the record of diagenesis, local redox conditions, and global seawater chemistry during the latest Ordovician glaciation. *Earth Planet. Sci. Lett.* 459:145–56

Algeo TJ, Berner RA, Maynard JB, Scheckler SE. 1995. Late Devonian Oceanic Anoxic Events and biotic crises: "Rooted" in the evolution of vascular land plants? GSA Today 5: 45

Algeo TJ, Ingall E. 2007. Sedimentary C_{org}:P ratios, paleocean ventilation, and Phanerozoic atmospheric pO_2. Palaeogeography Palaeoclimatology Palaeoecology 256: 130-55

Arvidson RS, Mackenzie FT, Guidry MW. 2013. Geologic history of seawater: A MAGic approach to carbon chemistry and ocean ventilation. Chemical Geology 362: 287-304

Bambach RK. 2006. Phanerozoic biodiversity mass extinctions. Annual Review of Earth and Planetary Sciences 34: 127-55

Beerling DJ, Lake JA, Berner RA, Hickey LJ, Taylor DW, Royer DL. 2002. Carbon isotope evidence implying high O_2/CO_2 ratios in the Permo-Carboniferous atmosphere. Geochimica et Cosmochimica Acta 66: 3757–67

Belcher CM, McElwain JC. 2008. Limits for combustion in low O_2 redefine paleoatmospheric predictions for the Mesozoic. Science 321: 1197-200

Belcher, CM, Collinson, ME Scott, AC. 2013. A 450-million-year history of fire. In *Fire Phenomena and the Earth System*, ed. CM Belcher, pp. 229–249. Chichester: Wiley-Blackwell

Benton MJ, Twitchett RJ. 2003. How to kill (almost) all life: the end-Permian extinction event. Trends in Ecology & Evolution 18: 358-65

Bergman NM, Lenton TM, Watson AJ. 2004. COPSE: A new model of biogeochemical cycling over Phanerozoic time. American Journal of Science 304: 397-437

Berner RA. 1987. Models for carbon and sulfur cycles and atmospheric oxygen: application to Paleozoic geologic history. American Journal of Science 287: 177-96

Berner EK, Berner RA. 1987. The global water cycle: geochemistry and environment. Prentice-Hall, Englewood Cliffs, NJ, USA.

Berner RA. 1991. A model for atmospheric CO_2 over Phanerozoic time. American Journal of Science 291: 339-76

Berner RA. 2001. Modeling atmospheric O_2 over Phanerozoic time. Geochimica et Cosmochimica Acta 65: 685-94

Berner RA. 2004. The Phanerozoic Carbon Cycle: CO_2 and O_2. Oxford: Oxford University Press

Berner RA. 2006. GEOCARBSULF: A combined model for Phanerozoic atmospheric O_2 and CO_2. Geochimica et Cosmochimica Acta 70: 5653-64

Berner RA. 2009. Phanerozoic atmospheric oxygen: new results using the GEOCARBSULF model. American Journal of Science 309: 603-6

Berner RA, Petsch ST, Lake JA, Beerling DJ, Popp BN, et al. 2000. Isotope fractionation and atmospheric oxygen: implications for Phanerozoic O_2 evolution. Science 287: 1630-33

Berner RA, Canfield DE. 1989. A new model for atmospheric oxygen over Phanerozoic time. American Journal of Science 289: 333-61

Berner RA, Kothavala Z. 2001. Geocarb III: A revised model of atmospheric CO2 over Phanerozoic time. American Journal of Science 301: 182-204

Blamey NJF, Brand U, Parnell J, Spear N, Lécuyer C, et al. 2016. Paradigm shift in determining Neoproterozoic atmospheric oxygen. Geology 44: 651-4

Blamey NJF, Brand U. 2019. Atmospheric gas in modern and ancient halite fluid inclusions: A screening protocol. Gondwana Research 69: 163-76

Brand U, Davis AM, Shaver KK, Blamey NJF, Heizler M, Lécuyer C. 2021. Atmospheric oxygen of the Paleozoic. Earth-Science Reviews 216:103560

Brune S, Williams SE, Müller RD. 2017. Potential links between continental rifting, CO_2 degassing and climate change through time. Nature Geoscience 10: 941-6

Budyko MI, Ronov AB, Yanshin AL. 1987. History of Earth's atmosphere. Berlin. Springer-Verlag.

Buick R. 2008. When did oxygenic photosynthesis evolve? Philos. Trans. R. Soc. Lond. B Biol. Sci. 363: 2731-43

Canfield DE. 1998. A new model for Proterozoic ocean chemistry. Nature 396: 450-3

Canfield DE. 2014. Proterozoic atmospheric oxygen. Treatise on Geochemistry 6: 197-216

Canfield DE, Teske A. 1996. Late Proterozoic rise in atmospheric oxygen concentration inferred from phylogenetic and sulphur-isotope studies. Nature 382: 127-32

Cannell A, Blamey N, Brand U, Escapa I, Large R. 2022. A revised sedimentary pyrite proxy for atmospheric oxygen in the Paleozoic: Evaluation for the Silurian-Devonian-Carboniferous period and the relationship of the results to the observed biosphere record. Earth-Science Reviews 231: 104062

Catling DC, Zahnle KJ. 2000. The Archean Atmosphere. Science Advances 6:eaax1420

Chaboureau AC, Sepulchre P, Donnadieu Y, Franc A. 2014. Tectonic-driven climate change and the diversification of angiosperms. Proc Natl Acad Sci U S A 111: 14066-70

Chu D, Grasby SE, Song H, Dal Corso J, Wang Y, et al. 2020. Ecological disturbance in tropical peatlands prior to marine Permian-Triassic mass extinction. Geology 48: 288-92

Cope MJ, Chaloner WG. 1980. Fossil charcoal as evidence of past atmospheric composition. Nature 283: 647-9

Cramer BD, Jarvis I. 2020. Carbon isotope stratigraphy. In Geologic Time Scale 2020, eds FM Gradstein, JG Ogg, M Schmitz, G Ogg, pp. 309–343. Amsterdam: Elsevier

Crockford PW, Kunzmann M, Bekker A, Hayles J, Bao H, et al. 2019. Claypool continued: Extending the isotopic record of sedimentary sulfate. Chemical Geology 513: 200-25

Dahl TW, Hammarlund EU, Anbar AD, Bond DPG, Gill BC, et al. 2010. Devonian rise in atmospheric oxygen correlated to the radiations of terrestrial plants and large predatory fish. PNAS 107: 17911-5

Dahl TW, Hammarlund EU. 2011. Do large predatory fish track ocean oxygenation? Commun Integr Biol 4: 92-4

Daines SJ, Mills BJ, Lenton TM. 2017. Atmospheric oxygen regulation at low Proterozoic levels by incomplete oxidative weathering of sedimentary organic carbon. Nat Commun 8: 14379

Dal Corso J, Mills BJW, Chu D, Newton RJ, Mather TA, et al. 2020. Permo-Triassic boundary carbon and mercury cycling linked to terrestrial ecosystem collapse. Nat Commun 11: 2962

Diefendorf AF, Freeman KH, Wing SL. 2012. Distribution and carbon isotope patterns of diterpenoids and triterpenoids in modern temperate C3 trees and their geochemical significance. Geochimica et Cosmochimica Acta 85: 342-56

Diessel CF. 2010. The stratigraphic distribution of inertinite. International Journal of Coal Geology 81: 251–268.

Domeier M, Torsvik TH. 2017. Full-plate modelling in pre-Jurassic time. Geological Magazine 156: 261-80

Edwards CT. 2019. Links between early Paleozoic oxygenation and the Great Ordovician Biodiversification Event (GOBE): A review. Palaeoworld 28: 37-50

Edwards CT, Saltzman MR, Royer DL, Fike DA. 2017. Oxygenation as a driver of the Great Ordovician Biodiversification Event. Nature Geoscience 10: 925-9

874 Engbretson DC, Kelley KP, Cashman HJ, Richards MA. 1992. 180 Million years of subduction. GSA
875 Today 2: 93-100

876 Erwin D. H. 1993. The Great Paleozoic Crisis. Life and Death in the Permian. Critical Moments in
877 Paleobiology and Earth History Series. New York: Columbia University Press.

878 Extier T, Landais A, Bréant C, Prié F, Bazin L, et al. 2018. On the use of δ^{18}Oatm for ice core dating.
879 Quaternary Science Reviews 185: 244-57

880 Falkowski PG, Katz ME, Milligan AJ, Fennel K, Cramer BS, et al. 2005. The rise of oxygen over the
881 past 205 million years and the evolution of large placental mammals. Science 309: 2202-4

882 Farquhar J, Bao H, Thiemens M. 2000. Atmospheric influence of Earth's earliest sulphur cycle. Science
883 289: 756-8

884 Fielding CR, Frank TD, McLoughlin S, Vajda V, Mays C, et al. 2019. Age and pattern of the southern
885 high-latitude continental end-Permian extinction constrained by multiproxy analysis. Nat
886 Commun 10: 385

887 Franz HB, Trainer MG, Malespin CA, Mahaffy PR, Atreya SK, et al. 2017. Initial SAM calibration gas
888 experiments on Mars: Quadrupole mass spectrometer results and implications. Planetary and
889 Space Science 138: 44-54

890 Gaffin S. 1987. Ridge volume dependence on seafloor generation rate and inversion using long term
891 sealevel change. American Journal of Science 287: 596-611

892 Garrels RM, Lerman A. 1984. Coupling the sedimentary sulfur and carbon cycles - an improved model.
893 American Journal of Science 284: 989-1007

894 Garrels RM, Perry EA. 1974. Cycling of C, S and O through geologic time. In The Sea, ed. ED Goldberg
895 pp. 303-36. New York: Wiley-Interscience

896 Glasspool IJ, Scott AC, Waltham D, Pronina N, Shao L. 2015. The impact of fire on the Late Paleozoic
897 Earth system. Front Plant Sci 6: 756

898 Glasspool IJ, Gastaldo RA. 2022. Silurian wildfire proxies and atmospheric oxygen. Geology. In press.

899 Glasspool IJ, Scott AC. 2010. Phanerozoic concentrations of atmospheric oxygen reconstructed from
900 sedimentary charcoal. Nature Geoscience 3: 627-30

901 Gregory BS, Claire MW, Rugheimer S. 2021. Photochemical modelling of atmospheric oxygen levels
902 confirms two stable states. Earth and Planetary Science Letters 561, 116818

903 Gurung K, Field KJ, Batterman SA, Godderis Y, Donnadieu Y, et al. 2022. Climate windows of
904 opportunity for plant expansion during the Phanerozoic. Nat Commun 13: 4530

Hay WW, Migdisov A, Balukhovsky AN, Wold CN, Flögel S, Söding E. 2006. Evaporites and the salinity of the ocean during the Phanerozoic: Implications for climate, ocean circulation and life. Palaeogeography, Palaeoclimatology, Palaeoecology 240: 3-46

Hayes JM, Strauss H, Kaufman AJ. 1999 The abundance of ^{13}C in marine organic matter and isotopic fractionation in the global biogeochemical cycle of carbon during the past 800 Ma. Chemical Geology 161

He T, Zhu M, Mills BJW, Wynn PM, Zhuravlev AY, et al. 2019. Possible links between extreme oxygen perturbations and the Cambrian radiation of animals. Nature Geoscience 12:468–474

He T, Corso JD, Newton RJ, Wignall PB, Mills BJW, et al. 2020. An enormous sulfur isotope excursion indicates marine anoxia during the end-Triassic mass extinction. Science Advances 6: eabb6704

Hedges JI, Keil RG. 1995. Sedimentary organic matter preservation: an assessment and speculative synthesis. Marine Chemistry 49: 81-115

Holland HD. 2006. The oxygenation of the atmosphere and oceans. Phil. Trans. R. Soc. B 361: 903-15

Horscroft JA, Kotwica AO, Laner V, West JA, Hennis PJ, et al. 2017. Metabolic basis to Sherpa altitude adaptation. Proc Natl Acad Sci U S A 114: 6382-7

Jørgensen BB, Nelson DC. 2004. Sulfide Oxidation in marine sediments: Geochemistry meets microbiology. In Sulfur Biogeochemistry - Past and Present. eds JP Amend, KJ Edwards, TW Lyons, Geological Society of America Special Papers 379.

Kanzaki Y, Kump LR. 2017. Biotic effects on oxygen consumption during weathering: Implications for the second rise of oxygen. Geology 45: 611-614

Krause AJ, Mills BJW, Zhang S, Planavsky NJ, Lenton TM, Poulton SW. 2018. Stepwise oxygenation of the Paleozoic atmosphere. Nat Commun 9: 4081

Kump LR, Fallick AE, Melezhik VA, Strauss H, Lepland A. 2013. The Great Oxidation Event. In Reading the Archive of Earth's Oxygenation, pp. 1517-33 Berlin, Heidelberg:Springer

Large RR, Mukherjee I, Gregory D, Steadman J, Corkrey R, Danyushevsky LV. 2019. Atmosphere oxygen cycling through the Proterozoic and Phanerozoic. Mineralium Deposita 54: 485-506

Lenton TM, Daines SJ, Mills BJW. 2018. COPSE reloaded: An improved model of biogeochemical cycling over Phanerozoic time. Earth-Science Reviews 178: 1-28

Levin L. 2003. Oxygen minimum zone benthos: adaption and community response to hypoxia. In Oceanography and Marine Biology, An Annual Review, Volume 41. London. eds Gibson RN, Atkinson RJA.

936 Li G, Elderfield H. 2013. Evolution of carbon cycle over the past 100 million years. Geochimica et
937 Cosmochimica Acta 103: 11-25

938 Liu XM, Kah LC, Knoll AH, Cui H, Wang C, et al. 2021. A persistently low level of atmospheric
939 oxygen in Earth's middle age. Nat Commun 12: 351

940 Lyons TW, Reinhard CT, Planavsky NJ. 2014. The rise of oxygen in Earth's early ocean and
941 atmosphere. Nature 506: 307-15

942 Maloof AC, Porter SM, Moore JL, Dudas FO, Bowring SA, Higgins JA, Fike DA, Eddy MP. 2010. The
943 earliest Cambrian record of animals and ocean geochemical change. Geological Society of
944 America Bulletin. 122, 1731–1774.

945 Mills DB, Ward LM, Jones C, Sweeten B, Forth M, et al. 2014. Oxygen requirements of the earliest
946 animals. Proc Natl Acad Sci U S A 111: 4168-72

947 Mills BJW, Scotese CR, Walding NG, Shields GA, Lenton TM. 2017. Elevated CO_2 degassing rates
948 prevented the return of Snowball Earth during the Phanerozoic. Nat Commun 8: 1110

949 Mills BJW, Krause AJ, Scotese CR, Hill DJ, Shields GA, Lenton TM. 2019. Modelling the long-term
950 carbon cycle, atmospheric CO_2, and Earth surface temperature from late Neoproterozoic to
951 present day. Gondwana Research 67: 172-86

952 Mills BJW, Donnadieu Y, Goddéris Y. 2021. Spatial continuous integration of Phanerozoic global
953 biogeochemistry and climate. Gondwana Research 100: 73-86

954 Otto-Bliesner BL. 1995. Continental drift, runoff and weathering feedbacks: Implications from climate
955 model experiments. Journal of Geophysical Research 100: 11537-48

956 Payne JL, Boyer AG, Brown JH, Finnegan S, Kowalewski M, et al. 2009. Two-phase increase in the
957 maximum size of life over 3.5 billion years reflects biological innovation and environmental
958 opportunity. PNAS 106: 24-7

959 Petit J-R, Raynaud D. 2020. Forty years of ice-core records of CO_2. Nature 579: 505-6

960 Pohl A, Ridgwell A, Stockey RG, Thomazo C, Keane A, et al. 2022. Continental configuration controls
961 ocean oxygenation during the Phanerozoic. Nature 608: 523-7

962 Poulton SW, Bekker A, Cumming VM, Zerkle AL, Canfield DE, Johnston DT. 2021. A 200-million-
963 year delay in permanent atmospheric oxygenation. Nature 592: 232-6

964 Poulton SW, Canfield DE. 2005. Development of a sequential extraction procedure for iron:
965 implications for iron partitioning in continentally derived particulates. Chemical Geology 214:
966 209-21

967 Pyne SJ, Andrews PL, Laven RD. 1996. *Introduction to Wildland Fire* (2nd edn). New York: Wiley.
968 769 pp.

969 Rasmussen B, Buick R. 1999. Redox state of the Archean atmosphere: evidence from detrital heavy
970 minerals in ca. 3250–2750 Ma sandstones from the Pilbara Craton, Australia. Geology 27:115-8.

971 Redfield AC. 1958. The biological control of chemical factors in the environment. American Scientist
972 46: 205-21

973 Ronov AB. 1976. Global carbon geochemistry, volcanism, carbonate accumilation, and life.
974 Geochemistry International 13: 172-95

975 Ronov AB. 1993. Stratisfera—Ili Osadochnaya Obolochka Zemli (Kolichestvennoe Issledovanie).
976 Moskva

977 Royer DL, Donnadieu Y, Park J, Kowalczyk J, Godderis Y. 2014. Error analysis of CO_2 and O_2
978 estimates from the long-term geochemical model GEOCARBSULF. American Journal of
979 Science 314: 1259-83

980 Royer DL. 2016. Climate sensitivity in the geologic past. Annual Review of Earth and Planetary
981 Sciences 44: 277-93

982 Saltzman MR, Thomas E. 2012. Carbon isotope stratigraphy. In The Geologic Time Scale 2012, eds F
983 Gradstein, J Ogg, M Schmitz, G Ogg, pp. 207–232 Amsterdam: Elsevier.

984 Schachat SR, Labandeira CC, Saltzman MR, Cramer BD, Payne JL, Boyce CK. 2018. Phanerozoic pO_2
985 and the early evolution of terrestrial animals. Proc Biol Sci 285

986 Scott AC. 1989. Observations on the nature and origin of fusain. International Journal of Coal Geology:
987 12, 443-475.

988 Scott, A. C. & Glasspool, I. J. 2007. Observations and experiments on the origin and formation of
989 inertinite group macerals. Int. J. Coal Geol. 70, 53–66.

990 Scott AC and Jones TP. 1991. Microscopical observations of recent and fossil charcoal: Microscopy
991 and Analysis 25: 13-15.

992 Servais T, Harper DAT. 2018. The Great Ordovician Biodiversification Event (GOBE): definition,
993 concept and duration. Lethaia 51: 151-64

994 Sim MS, Bosak T, Ono S. 2011. Large sulfur isotope fractionation does not require disproportionation.
995 Science 333: 74-7

996 Sonderholm F, Bjerrum CJ. 2021. Minimum levels of atmospheric oxygen from fossil tree roots imply
997 new plant-oxygen feedback. Geobiology 19: 250-60

998 Sperling EA, Wolock CJ, Morgan AS, Gill BC, Kunzmann M, et al. 2015. Statistical analysis of iron
999 geochemical data suggests limited late Proterozoic oxygenation. Nature 523: 451-4

1000 Steadman JA, Large RR, Blamey NJ, Mukherjee I, Corkrey R, et al. 2020. Evidence for elevated and
1001 variable atmospheric oxygen in the Precambrian. Precambrian Research 343:105722

1002 Stolper DA, Bender ML, Dreyfus GB, Yan Y, Higgins JA. 2016. A Pleistocene ice core record of
1003 atmospheric O_2 concentrations. Science 353: 1427-30

1004 Sulej T, Krzesinski G, Talanda M, Wolniewicz AS, Blazejowski B, et al. 2020. The earliest-known
1005 mammaliaform fossil from Greenland sheds light on origin of mammals. Proc Natl Acad Sci U
1006 S A 117: 26861-7

1007 Tappert R, McKellar RC, Wolfe AP, Tappert MC, Ortega-Blanco J, Muehlenbachs K. 2013. Stable
1008 carbon isotopes of C3 plant resins and ambers record changes in atmospheric oxygen since the
1009 Triassic. Geochimica et Cosmochimica Acta 121: 240-62

1010 VanCappellen P, Ingall ED. 1994. Benthic phosphorus regeneration, net primary production, and ocean
1011 anoxia - a model of the coupled marine biogeochemical cycles of carbon and phosphorus.
1012 Paleoceanography 9: 677-92

1013 Wallace MW, Hood Av, Shuster A, Greig A, Planavsky NJ, Reed CP. 2017. Oxygenation history of the
1014 Neoproterozoic to early Phanerozoic and the rise of land plants. Earth and Planetary Science
1015 Letters 466: 12-9

1016 Watson AJ, Lenton TM, Mills BJW. 2017. Ocean deoxygenation, the global phosphorus cycle and the
1017 possibility of human-caused large-scale ocean anoxia. Philos Trans A Math Phys Eng Sci 375

1018 Wignall PB, Twitchett RJ. 1996. Oceanic anoxia and the end Permian mass extinction. Science 272:
1019 1155-8

1020 Wildman RA, Hickey LJ, Dickinson MB, Berner RA, Robinson JM, et al. 2004. Burning of forest
1021 materials under late Paleozoic high atmospheric oxygen levels. Geology 32: 457-60

1022 Wold CN, Hay WW. 1990. Estimating ancient sediment fluxes. Am. J. Sci. 290: 1069-1089

1023 Wood R, Liu AG, Bowyer F, Wilby PR, Dunn FS, et al. 2019. Integrated records of environmental
1024 change and evolution challenge the Cambrian Explosion. Nat Ecol Evol 3: 528-38

1025 Wu N, Farquhar J, Strauss H, Kim S-T, Canfield DE. 2010. Evaluating the S-isotope fractionation
1026 associated with Phanerozoic pyrite burial. Geochimica et Cosmochimica Acta 74: 2053-71

Xu Z, Hilton J, Yu J, Wignall PB, Yin H, et al. 2022. End Permian to Middle Triassic plant species richness and abundance patterns in South China: Coevolution of plants and the environment through the Permian–Triassic transition. Earth-Science Reviews 232

Yan Y, Brook EJ, Kurbatov AV, Severinghaus JP, Higgins JA. 2019. Ice core evidence for atmospheric oxygen decline since the Mid-Pleistocene transition. Science Advances 7: eabj9341

Zhang S, Planavsky NJ, Krause AJ, Bolton EW, Mills BJW. 2018. Model based Paleozoic atmospheric oxygen estimates: a recent visit to GEOCARBSULF. Am. J. Sci. 318: 557–589.

Zhao W, Zhang X, Jia G, Shen Y, Zhu M. 2021. The Silurian-Devonian boundary in East Yunnan (South China) and the minimum constraint for the lungfish-tetrapod split. Sci. China Earth Sci. 64: 1784–1797.

Terms and Definitions

Aerobic respiration:

The chemical process by which oxygen reacts with carbohydrates to generate energy.

Exoplanet:

A planet which is outside of our solar system. It may or may not orbit another star.

Inertinite:

Fossilised charcoal, usually derived from the pyrolysis of wood, but can sometimes contain the charred remains of seeds, flowers and fungal cells.

Halite:

Commonly known as rock salt, with the formula NaCl.

Acknowledgements

BJWM is funded by the UK Natural Environment Research Council (NE/S009663/1). AJK was funded by the NERC SPHERES Doctoral Training Partnership (NE/L002574/1).

Related resources

The combined O_2 estimate shown in Figure 6 is available to download as a dataset from https://github.com/bjwmills

The GEOCARBSULFOR model code is available to download at https://github.com/alexjkrause